

Electronic Supplementary Information

Isolated Ni single atoms in graphene nanosheets for high-performance CO₂ reduction

Kun Jiang, Samira Siahrostami, Tingting Zheng, Yongfeng Hu, Sooyeon Hwang, Eli Stavitski, Yande Peng, James Dynes, Mehesh Gangisetty, Dong Su, Klaus Attenkofer, and Haotian Wang*

*Corresponding author: H.W. (hwang@rowland.harvard.edu)

This ESI file includes:

- Fig. S1 Additional aberration-corrected HAADF-STEM image of Ni-NG nanosheet, together with EDX elemental mapping and zoom-in edge region.
- Fig. S2 XPS survey characterization of Ni-NG.
- Fig. S3 TEM image of Ni NPs supported on graphene nanosheets.
- Fig. S4 CO₂RR performance comparison between graphene supported Ni nanoparticles and Ni-NG catalysts.
- Fig. S5 Tafel slope analysis of CO evolution over Ni-NG catalyst.
- Fig. S6 Electrochemical double layer capacitance measurements for bare glassy carbon electrode and Ni-NG catalyst covered glassy carbon electrode.
- Fig. S7 Characterizations of Ni-NG after 20-h's continuous electrolysis under -0.64 V CO₂-to-CO overpotential.
- Fig. S8 Electrochemical CO₂RR performance comparison on N-G, Ni-N and Ni-NG catalysts casted glassy carbon electrode.
- Fig. S9 Electrochemical CO₂RR performance on Ni₃N/CFP control sample.
- Fig. S10 XPS survey spectra for as received graphene oxide and control sample of NG.
- Fig. S11 Aberration-corrected HAADF-STEM image of NG and corresponding EDX spectrum.
- Fig. S12 Core level XPS spectra of (A) Ni 2p and (B) N 1s regions.
- Fig. S13 Ni K-edge XANES spectra of Ni-NG with compared to Ni-G, NiPc, NiO and Ni metal references.
- Fig. S14 Schematic chemical structure of Ni phthalocyanine (Ni-PC).
- Fig. S15 STEM images of Ni-G and EXAFS comparison of Ni-NG, Ni-G and Ni NPs/G.
- Fig. S16 Additional CO₂RR performance screening on Mn-NG, Fe-NG and Cu-NG catalysts.
- Fig. S17 Electrocatalytic CO₂RR performance comparison between Co-NG and Ni-NG.
- Fig. S18 STEM image and EXAFS of Co-NG.
- Fig. S19 Free energy diagrams of CO₂ to CO conversion
- Table S1 Comparisons of Ni-NG catalyst with reported non-noble metal CO₂-to-CO electrocatalysts in water.

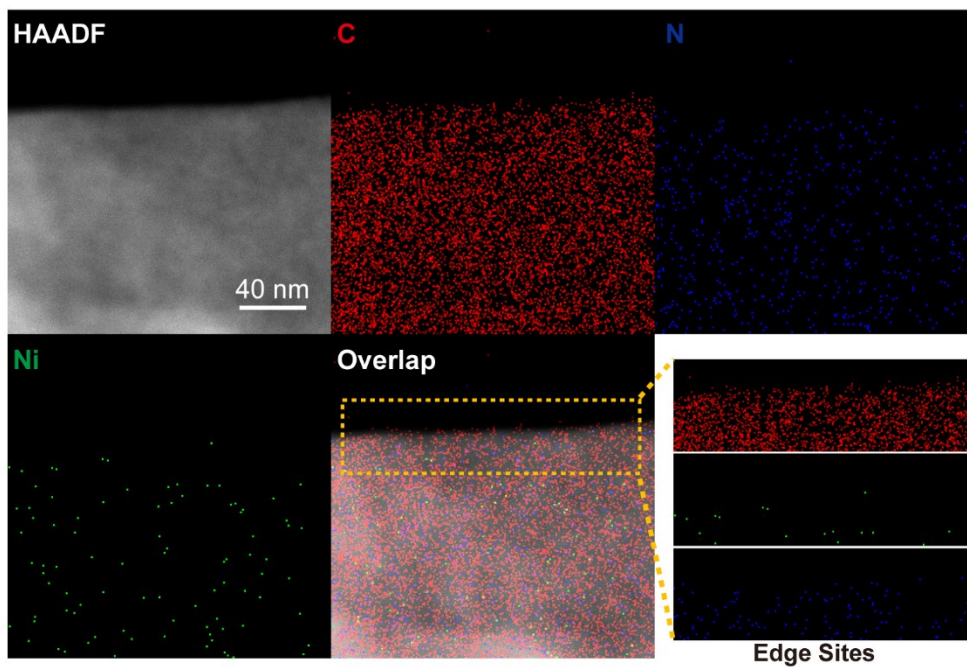


Fig. S1 Additional aberration-corrected HAADF-STEM image of Ni-NG nanosheet, together with EDX elemental mapping and zoom-in edge region.

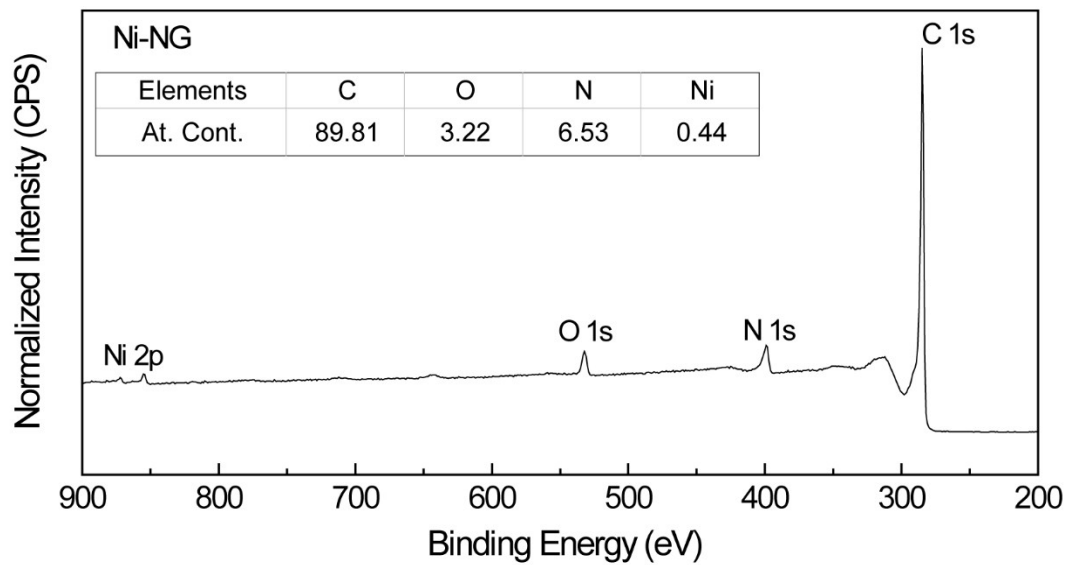


Fig. S2. XPS survey characterization of Ni-NG. Only C, O, N and Ni elements are detected and insert is their atomic content.

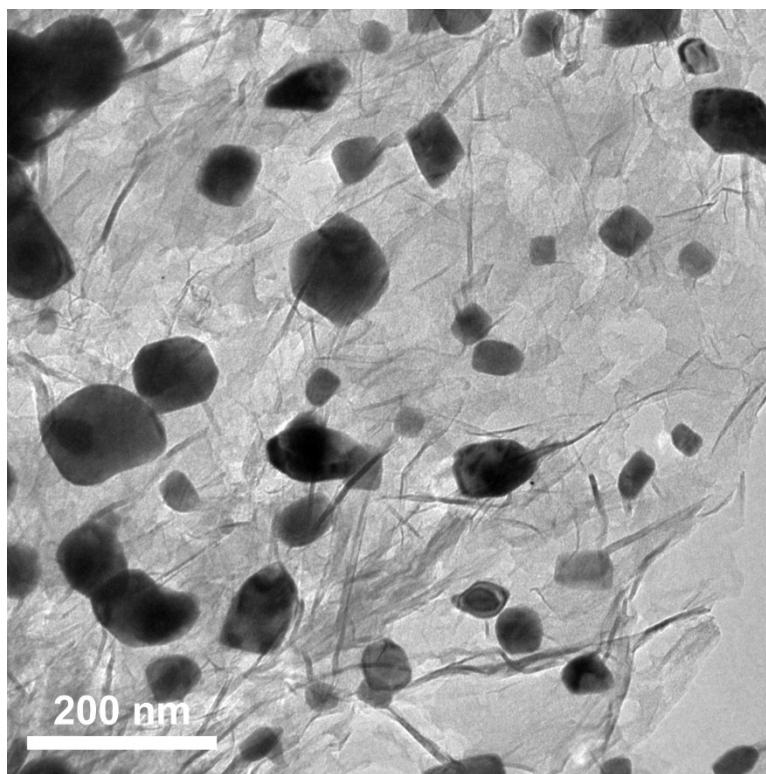


Fig. S3 TEM image of Ni NPs supported on graphene nanosheets.

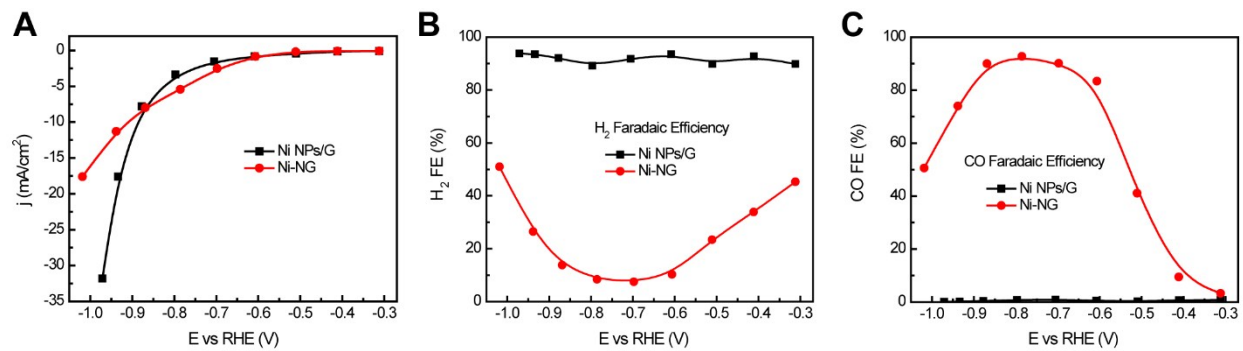


Fig. S4 CO₂RR performance comparison between graphene supported Ni nanoparticles and Ni-NG catalysts. (A) Overall steady state current densities, (B) H₂ Faradaic efficiencies and (C) CO Faradaic efficiencies recorded in CO₂ saturated 0.5 M KHCO₃ solution. H₂ is the predominant gas product observed on Ni nanoparticles.

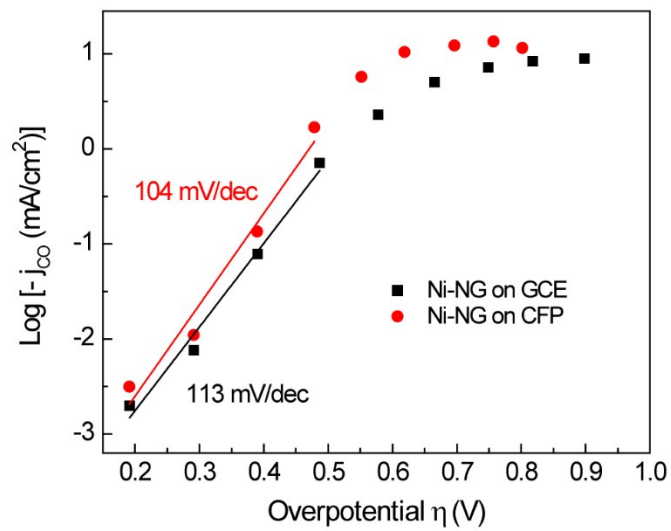


Fig. S5 Tafel slope analysis of CO evolution over Ni-NG catalyst casted onto either glassy carbon electrode or carbon fiber paper substrate.

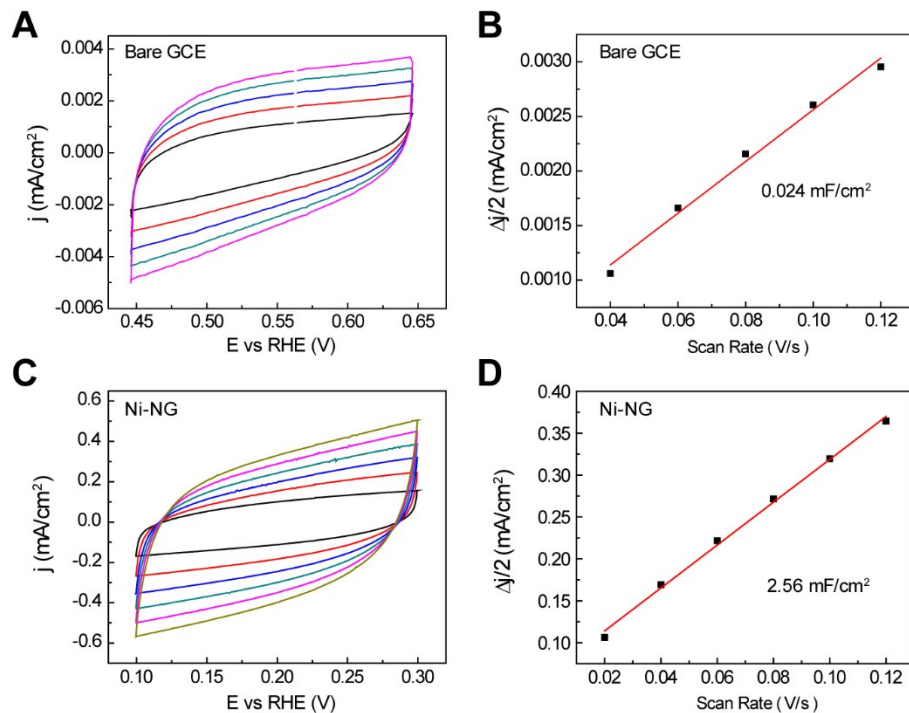


Fig. S6 Electrochemical double layer capacitance (EDLC) measurements for bare glassy carbon electrode and Ni-NG catalyst covered GCE.

The calculation of turnover frequency (TOF) per site was based on the estimation of the numbers of Ni active sites in Ni-NG catalyst. The determined EDLC of bare GCE substrate was $24 \mu\text{F}/\text{cm}^2$, close to the reported graphene value of $\sim 21 \mu\text{F}/\text{cm}^2$ (*J. Phys. Chem. Lett.* 2013, **4**, 1244-1253). We could estimate the electrochemical surface area of graphene layers in Ni-NG to be $\sim 122 \text{ cm}^2$ (or $\sim 61 \text{ m}^2/\text{g}$), given the $2.56 \text{ mF}/\text{cm}^2$ EDLC value of Ni-NG.

The moles of carbon atoms on the electrochemical surface can be calculated to be $122/10000 \text{ m}^2 / 2600 \text{ m}^2 \text{ g}^{-1} / 12 \text{ g mol}^{-1} = 3.9 \times 10^{-7} \text{ mol}$, where $2600 \text{ m}^2 \text{ g}^{-1}$ is the theoretical specific surface area of graphene (*J. Phys. Chem. Lett.* 2013, **4**, 1244-1253). Taken together the Ni atomic content in Ni-NG determined to be 0.44% by XPS (Fig. S2), the moles of Ni sites in the surface graphene layers is determined to be $\sim 1.7 \times 10^{-9} \text{ mol}$. The CO partial current on Ni-NG under an overpotential of 0.57 V is 2.3 mA, which gives us a TOF of Ni active site to be $2.3/1000 \text{ C s}^{-1} / 10^5 \text{ C mol}^{-1} / 2 / 1.7 \times 10^{-9} \text{ mol} = 6.8 \text{ s}^{-1}$ (or ca. 24350 h^{-1}) in H-cell, at an overpotential of 0.57 V; or likewise, ca. 21.2 s^{-1} at an overpotential of 0.75 V. Accordingly, the TOF of Ni site in MEA configuration is ca. 59 s^{-1} , with an cell voltage of 2.78 V (Fig. 3D).

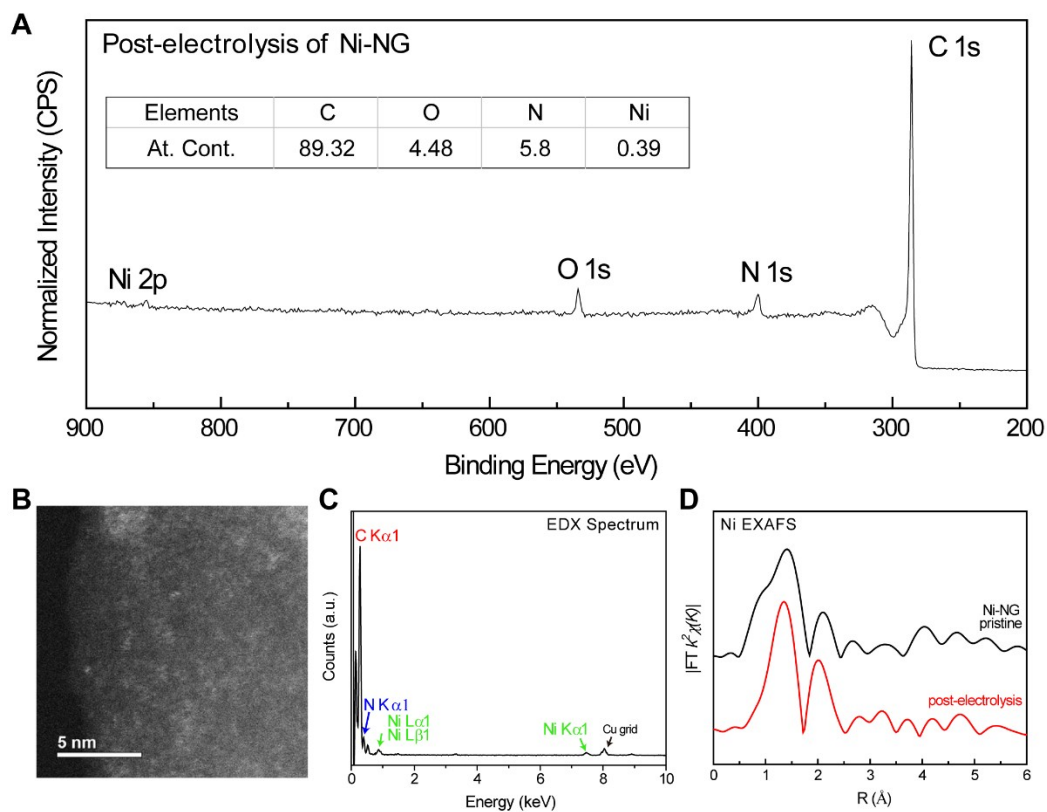


Fig. S7 Characterizations of Ni-NG after 20-h's continuous electrolysis under -0.64 V CO_2 -to-CO overpotential. (A) XPS survey, (B) STEM image and (C) corresponding EDX spectrum. The determined Ni:C ratio is close to that of pristine one, and no Ni NPs were observed after the long-term electrolysis. (D) EXAFS comparison of Ni-NG before and after the stability test, isolated Ni atom feature was largely maintained.

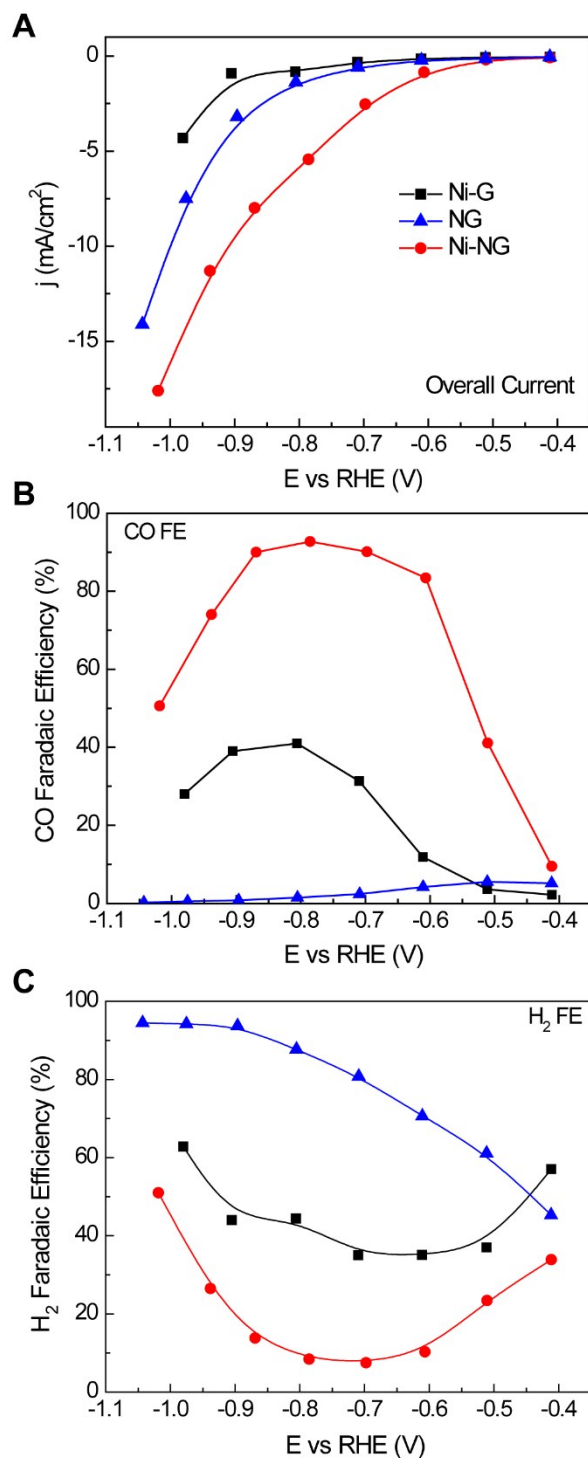


Fig. S8 Electrochemical CO₂RR performance comparison on N-G, Ni-N and Ni-NG catalysts casted glassy carbon electrode. N-G without any Ni-doping is predominant by HER during catalysis, while Ni-G shows a similar potential dependence of CO evolution with Ni-NG apart from the much lower FEs on the former.

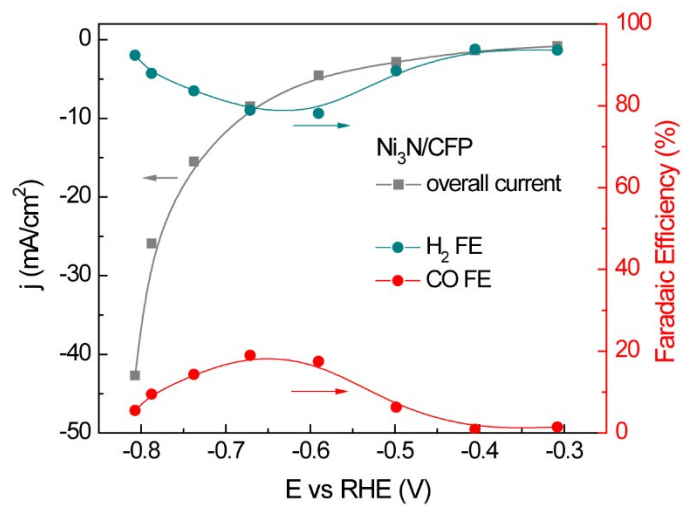


Fig. S9 Electrochemical CO₂RR performance on Ni₃N/CFP control sample, which delivers a maxima CO FE of ~ 19% at -0.67 V with a CO partial current of ~ 1.62 mA/cm².

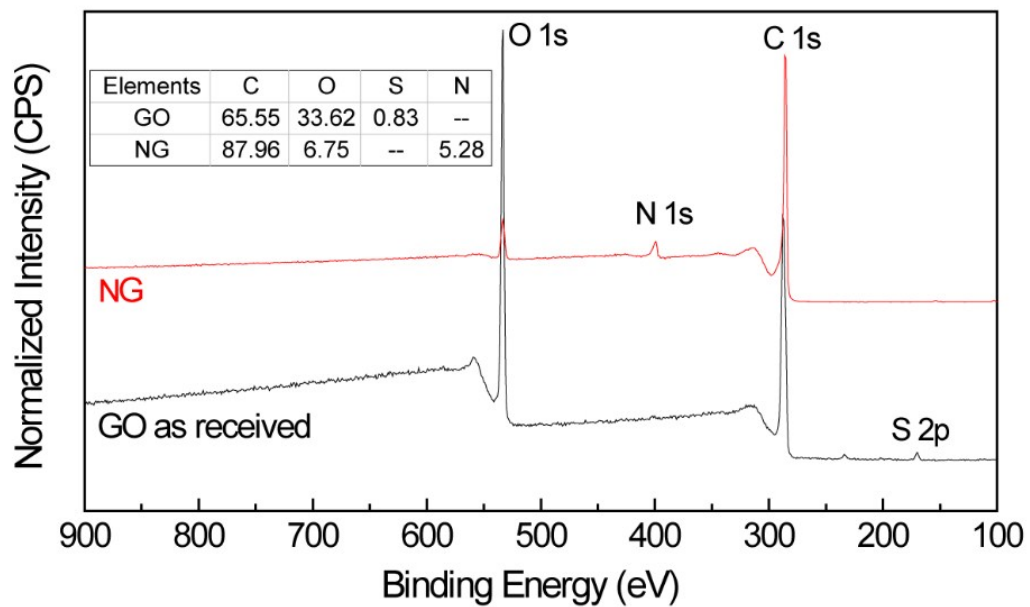


Fig. S10 XPS survey spectra for as-received graphene oxide (black line) and control sample of NG (red line), inset table shows the determined atomic percentage of each component.

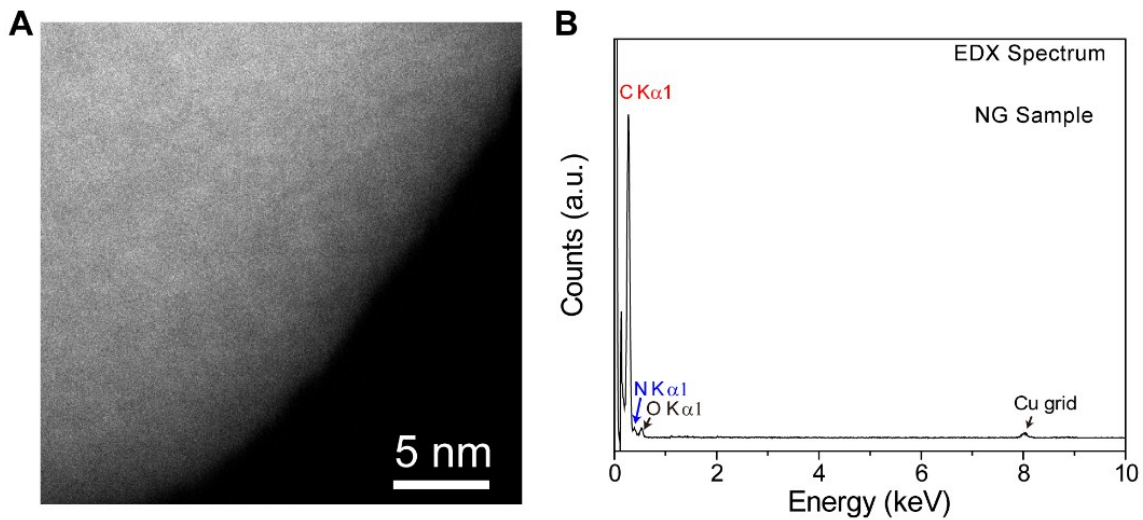


Fig. S11 Aberration-corrected HAADF-STEM image of NG and corresponding EDX spectrum. Neither bright dots of Ni atoms nor typical Ni peaks at 0.85 (Ni L α /L β) and 7.47 (Ni K α) were observed.

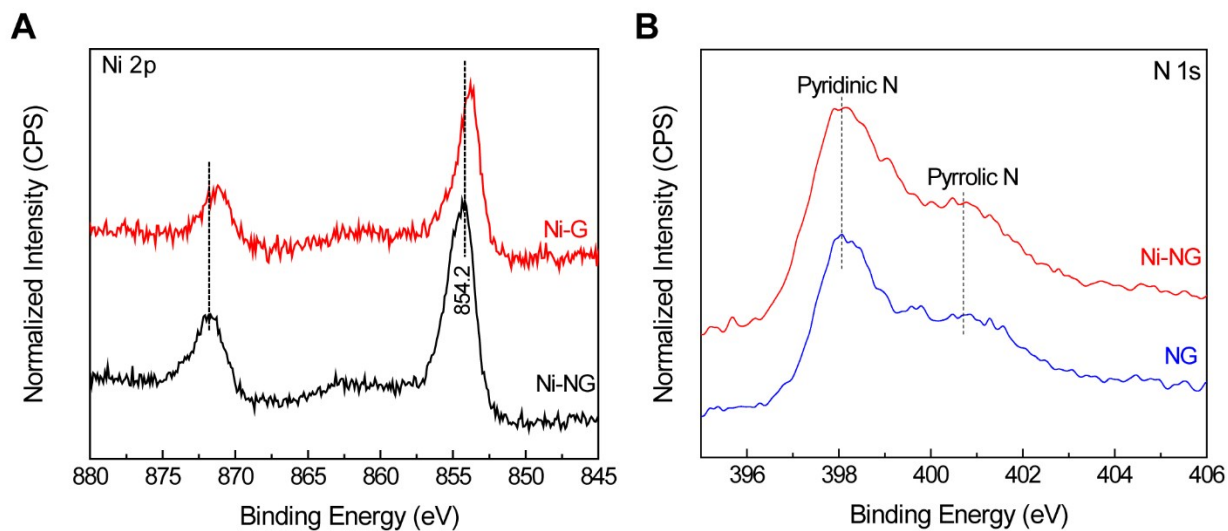


Fig. S12 Core level XPS spectra of (A) Ni 2p and (B) N 1s regions. The Ni 2p_{3/2} binding energy of Ni-G locates at 853.8 eV, which is more positive than that for Ni metal of 852.6 eV and corresponding to a partial oxidized status. Moreover, this Ni 2p binding energy shifts to higher values in Ni-NG sample at the presence of N, suggesting the possible Ni-N correlation and further discussion can be seen in main text together with XAS results.

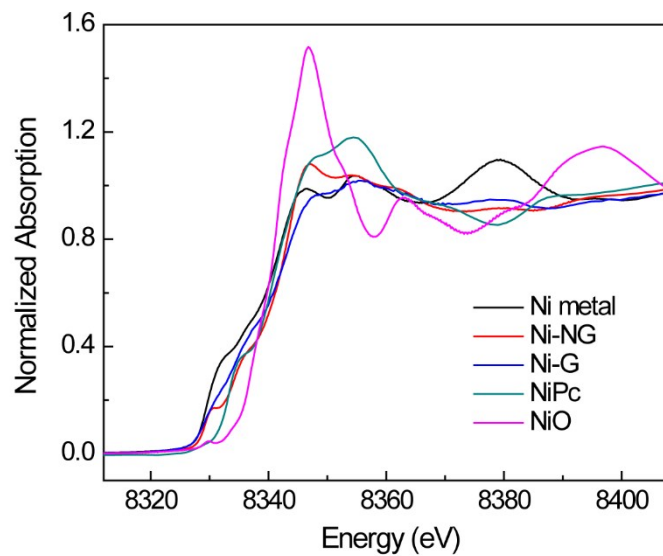


Fig. S13 Ni K-edge XANES spectra of Ni-NG with compared to Ni-G, NiPc, NiO and Ni metal references.

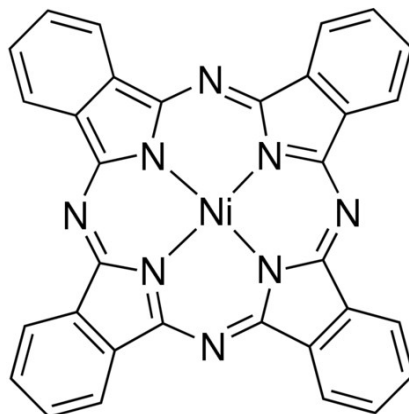


Fig. S14 Schematic chemical structure of Ni phthalocyanine (Ni-PC), where four Ni-N bonds are present and used as a reference for the chemical environment investigation of Ni-NG catalyst.

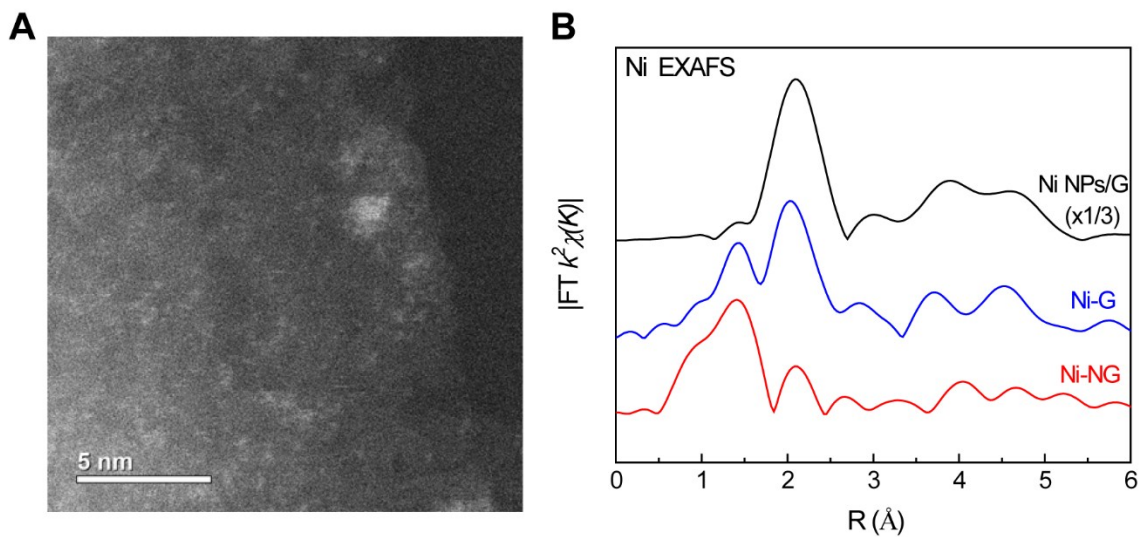


Fig. S15 (A) STEM images of Ni-G and (B) EXAFS comparison of Ni-NG, Ni-G and Ni NPs/G. In addition to Ni single atoms, there are some small Ni clusters observed, responsible for the relatively low CO selectivity.

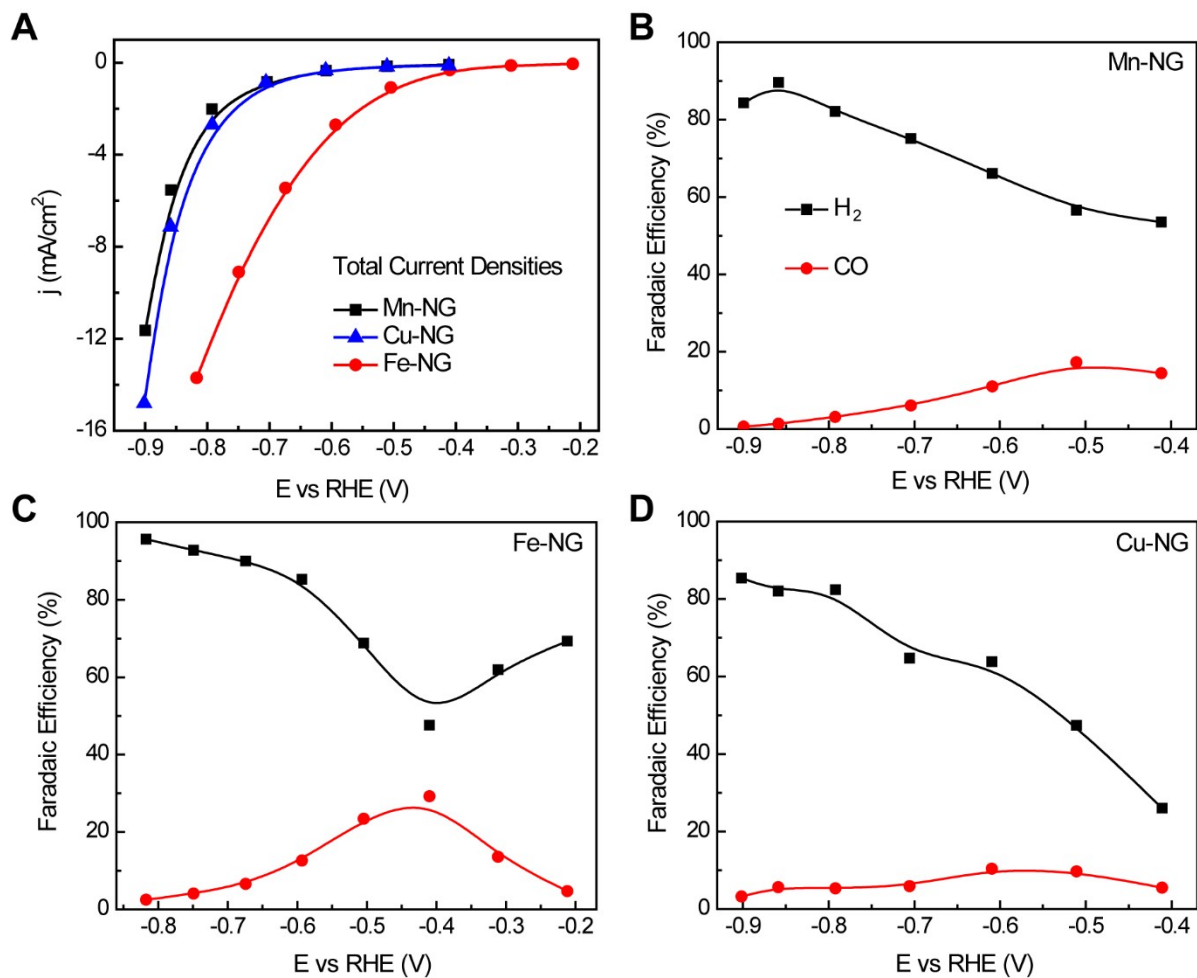


Fig. S16 Additional CO₂RR performance screening on Mn-NG, Fe-NG and Cu-NG catalysts. (A) Total current densities and (B-D) Faradaic efficiencies for detected gas products at different applied potentials on catalysts covered glassy carbon electrode (0.2 mg/cm² loading).

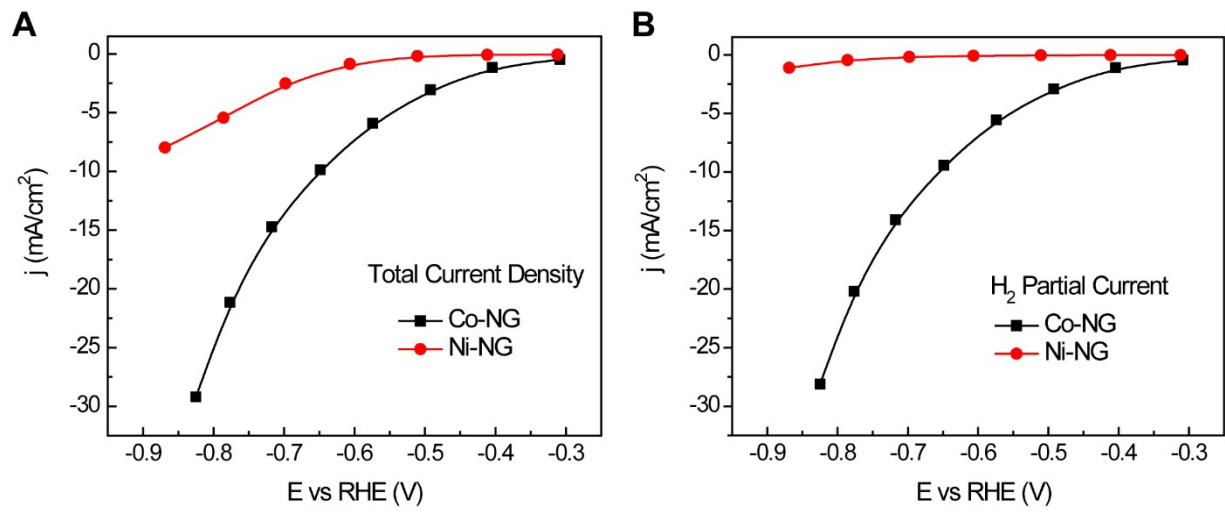


Fig. S17 Electrocatalytic CO₂RR performance comparison between Co-NG and Ni-NG. (A) Total current densities and (B) H₂ partial current densities recorded at different applied potentials on catalysts covered glassy carbon electrode (0.2 mg/cm² loading).

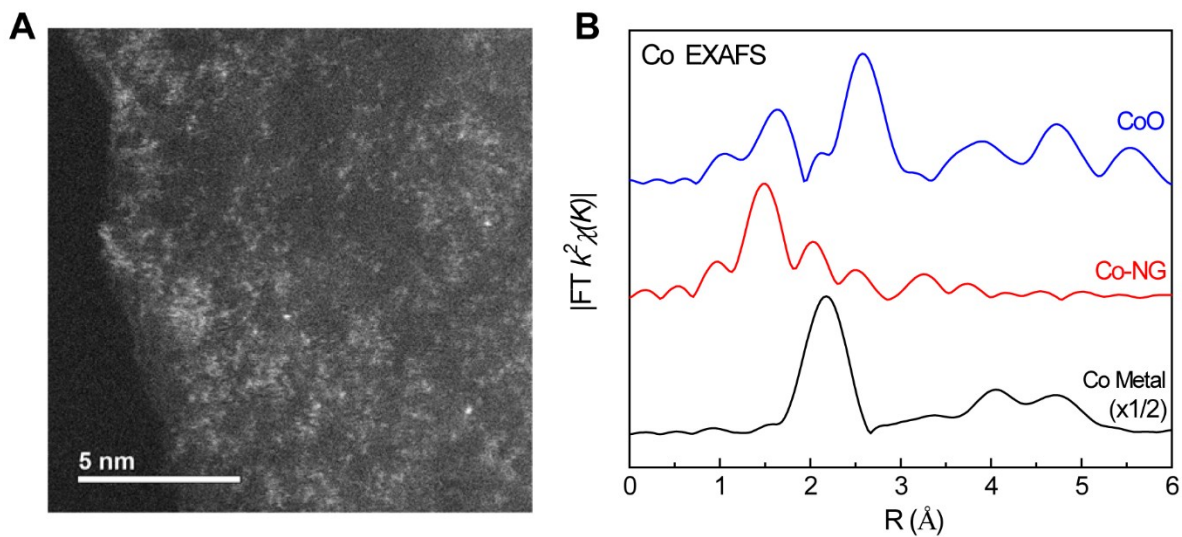


Fig. S18 (A) STEM image and (B) EXAFS of Co-NG. The Co single atoms were uniformly dispersed in graphene nanosheet, similar to the structure of Ni-NG. Different with Co metal which shows the feature peak at 2.17 \AA of Co-Co bonding, the predominant peak within Co-NG locates at ~ 1.50 \AA , ascribing to the Co-N/Co-C pair from isolated Co atoms [*Nat. Commun.*, 2015, 6, 8668].

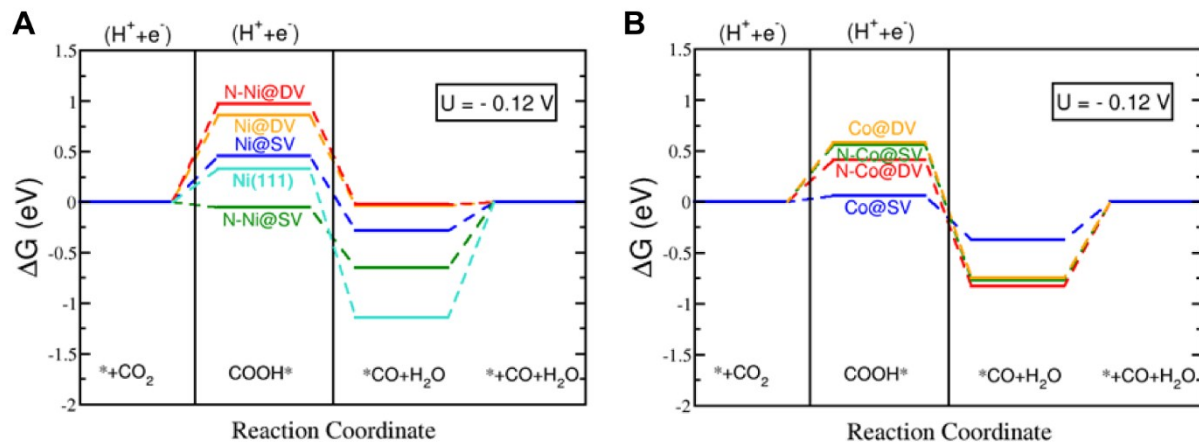


Fig. S19 Free energy diagrams of CO₂ to CO conversion on (A) Ni and (B) Co different examined active sites displayed in Figure 5A at equilibrium potential of -0.12 V vs. RHE.

Table S1 Comparisons of Ni-NG catalyst with reported non-noble metal CO₂-to-CO electrocatalysts in water.

Catalyst	CO FE (%)	j (mA/cm ²)	Overpotential (V)	Electrolyte	Reference
Ni-NG	95.0	11	0.62	0.5M KHCO₃	This work
Ni-NG (MEA)	97.0	51.5	N/A	0.1M KHCO₃	This work
Cu/Ni(OH) ₂	92	4.3	0.39	0.5M NaHCO ₃	<i>Sci. Adv.</i> 3 , e1701069 (2017)
CuO/SnO ₂	90	1.2	0.58	0.1M NaHCO ₃	<i>Nat. Energy</i> 2 , 17087 (2017)
COF-367-Co (1%) (Co porphyrin)	53	1.35	0.55	0.5M KHCO ₃	<i>Science</i> 349 , 1208 (2015)
COF-367-Co	91	13.2	0.55	0.5M KHCO ₃	<i>Science</i> 349 , 1208 (2015)
CoPc/CNT (2.5%)	92	10	0.51	0.1M KHCO ₃	<i>Nat. Commun.</i> 8 , 14675 (2017)
FeMn-N-C	84	1.8	0.40	0.1M KHCO ₃	<i>Angew. Chem.</i> 54 , 10758 (2015)
ZIF derived Fe _{0.5} d	91	7.5	0.48	0.1M NaHCO ₃	<i>ACS Catal.</i> 7 , 1520 (2017)
Ni-N-Gr	90	2	0.58	0.1M KHCO ₃	<i>Small</i> 12 , 6083 (2016)
NiN-GS	93.2	4.2	0.70	0.1M KHCO ₃	<i>Chem</i> 3 , 950 (2017)
Ni ₂ -CPDpy973(1)	87	0.55	0.78	0.1M KHCO ₃	<i>Nat. Commun.</i> 8 , 109 (2017)
Ni-N _x -C	85	9.5	0.66	0.1M KHCO ₃	<i>Nat. Commun.</i> 8 , 944 (2017)
Ni SAs/N-C	70.3	10.48	0.89	0.5M KHCO ₃	<i>J. Am. Chem. Soc.</i> 139 , 8078 (2017)